Improvement of aqueous solution coexisting with arsenite and arsenate using iron mixed porous clay pellets in batch and fixed-bed column studies

Nguyen Chi Thanh, Boonchai Wichitsathian, Chatpet Yossapol, Watcharapol Wonglertarak and Borano Te

ABSTRACT

Arsenic-polluted water is a global concern and puts millions of people at risk of developing cancer. The improvement of aqueous solution coexisting with arsenite and arsenate using iron mixed porous clay pellets was investigated in batch and fixed-bed column systems. Batch studies showed that the removal rate occurred in two main phases with an equilibrium time of 52 h. The pseudo-second-order model well described the experimental data. Isotherm data were well fitted by the Langmuir–Freundlich model. The removal efficiency was significantly reduced in alkaline solution and the presence of phosphate ions. The column study revealed that the breakthrough time and saturation time increased with lower feeding flow rate, higher bed height, and lower initial adsorbate concentration. The Thomas model provided good performance for predicting the column experimental data.

Key words | adsorbent, adsorption, breakthrough curve, fixed-bed column, kinetics

Nguyen Chi Thanh
Faculty of Applied Sciences,
Ton Duc Thang University,
Ho Chi Minh City,
Vietnam

Boonchai Wichitsathian
Chatpet Yossapol
Watcharapol Wonglertarak
Borano Te (corresponding author)
School of Environmental Engineering, Institute of Engineering,
Suranaree University of Technology,
Nakhon Ratchasima 30000,
Thailand
E-mail: *teborano12@gmail.com*

Borano Te
Faculty of Civil Engineering,
Preah Kossomak Polytechnic Institute,
Phnom Penh,
Cambodia

INTRODUCTION

Access to safe and clean drinking water is a prerequisite for a healthy life. Recently, many water sources around the globe have deteriorated due to the presence of excessive toxins and pathogens. One of the highly toxic and carcinogenic pollutants is arsenic. Concentrations greater than the World Health Organization guideline of 10 μg/L for arsenic in drinking water have been reported in 105 countries and expose a population of over 200 million (Chakraborti *et al.* 2017). Health problems associated with an excessive and long-term exposure to arsenic are skin problems, skin cancers, internal cancers (bladder, kidney, and lung), leg and foot blood-vessel diseases, reproductive disorders, adverse pregnancy outcomes, and intellectual malfunction in children (Sharma *et al.* 2014). In natural water, arsenic mainly presents in the forms of arsenite [As(III)] and arsenate [As(V)]. Therefore, it is necessary to treat As(III)- and As(V)-contaminated water via an affordable purification technique.

Adsorption is an advantageous technique in terms of simplicity, economy, removal efficiency, ease of operation and maintenance, flexibility to be scaled up (from the point of use to a community-based treatment plant), and avoidance of liquid waste generation on site (Sabbatini *et al.* 2010). Clay has gained much attention for use in removing pollutants such as metal ions, organic pollutants and bacteria due to its large specific surface area, chemical and mechanical stability, layer structure, and high cation exchange capacity (Sdiri *et al.* 2011). However, clay is difficult to apply in column adsorption due to its fine particle size, which creates a permeability problem (Mohapatra *et al.* 2007). To improve the adsorption capacity and permeability, clay can be modified or used as a binder to iron oxides, iron particles,

doi: 10.2166/ws.2019.069

or other metal oxides. Doušová *et al.* (2006) modified some clay minerals with iron salts to adsorb arsenic from aqueous solution and found that the sorption capacity increased from about 0.5 mg/g to around 20 mg/g. Bhowmick *et al.* (2014) indicated that montmorillonite-supported nanoscale zero-valent iron expressed an arsenic adsorption capacity of more than 45 mg/g, much higher than the 0.64 mg/g of montmorillonite found by Mohapatra *et al.* (2007).

Most previous studies, however, focused only on using a specific pure clay mineral such as kaolinite, montmorillonite, illite and smectite as a direct adsorbent or iron-modified clay mineral adsorbent for treating either As(III) or As(V) from water, and which was mostly performed in a batch mode. Research that completely addresses the use of natural clay for hosting iron species to simultaneously remove As(III) and As(V) from water in both batch and column systems is still limited. Therefore, this research aims to utilize iron mixed porous clay pellets (IMCP) to enhance the quality of water coexisting with As(III) and As(V) in batch and continuous column experiments.

MATERIALS AND METHODS

Materials and reagents

Natural clay (NC) was manually collected, dried, crushed, and sieved to be less than 75 μm in particle size. Iron oxide powder (Fe_2O_3) and iron powder (IP) were of analytical grade and industrial grade, respectively. Rice bran powder (RB) was obtained from a local grinding mill. To have the 100 mg/L of [50% As(III) + 50% As(V)] stock solution, the appropriate amounts of $Na_2HAsO_4{\cdot}7H_2O$ and $NaAsO_2$ (Sigma Aldrich) were dissolved together into deionized (DI) water. $NaNO_3$, Na_2SO_4, and Na_3HPO_4 were for the effect of the coexisting anions.

Adsorbent preparation

The detailed procedure for preparing IMCP was mentioned in our previous study (Te *et al.* 2017). Briefly, IMCP adsorbent was developed by mixing NC (52.15%), Fe_2O_3 (19.22%), IP (28.63%) and RB (15%). The prepared constituents were uniformly mixed along with the addition of DI water to produce a paste form. The paste was strongly stirred by hand for about 5–10 min and dried at 104 ± 1 °C for 24 h, and further heated at 600 °C for 2–3 h in a muffle furnace. After cooling down, the product was sieved for the desired particle size of 0.6–1.18 mm. The final product was kept in a dry and clean container for further experiments.

Batch experiments

A series of reactions between 10 g/L of IMCP and 0.5 mg/L of the adsorbate solution (pH = 7 ± 0.1) was prepared and shaken by a horizontal mechanical shaker with 150 rpm at room temperature (25 ± 1 °C) to observe the effect of contact time. The effect of initial concentration was performed by varying the adsorbate concentration from 0.1 to 100 mg/L. The effect of initial solution pH was conducted by varying pH from 3 to 11. The effect of coexisting anions was investigated by introducing 0.1, 1 and 10 mM of $NaNO_3$, Na_2SO_4 and Na_3HPO_4 into the 0.5 mg/L arsenic stock solution. Each sample was filtered through 0.22 μm syringe filters, acidified, kept at 4 °C and analyzed for arsenic concentration within 24 h. The adsorption capacity, Q_e (mg/g), and efficiency, R (%), were determined by Equations (1) and (2), respectively:

$$Q_e = \frac{(C_o - C_e)}{M} \times V \quad (1)$$

$$R(\%) = \frac{(C_o - C_e)}{C_o} \times 100 \quad (2)$$

where C_o (mg/L) and C_e (mg/L) are the initial and equilibrium adsorbate concentrations, respectively. V (L) is the volume of adsorbate solution, and M (g) is the mass of adsorbent.

Fixed-bed column experiments

The column experiments were conducted in polyethylene columns of 4.1 cm inner diameter and 31 cm height. The influent solution was introduced upward by peristaltic pumps (Watson-Marlow 505S, USA). The experimental conditions included the influent feed flow rates (12.5, 17, 20.5 mL/min), adsorbent bed heights (5, 10, 15 cm), and initial adsorbate concentrations (0.5, 1, 2 mg/L). The

adsorption capacity of IMCP at the breakthrough and saturation points could be calculated using Equation (3):

$$q_t = \frac{QC_o}{M}\int_0^t \left(1 - \frac{C_t}{C_o}\right)dt \quad (3)$$

where Q (mL/min) is the volumetric flow rate, M (g) is the mass of adsorbent packed in the column, and $\int_0^t (1 - \frac{C_t}{C_o})dt$ is the numerical integration of the area above the breakthrough curve.

Analytical methods

Arsenic concentration was measured by inductively coupled plasma–optical emission spectrometry (ICP-OES) (Optima 8000DV, PerkinElmer) using a wavelength of 193.7 nm. The surface area, total pore volume, and average pore diameter were obtained from the Brunauer–Emmett–Teller (BET) method using a BET analyzer (BELSORP Mini II, BEL Inc., Japan). X-ray diffraction (XRD) was performed using the Bruker XRD (D2 PHASER). The morphological features of IMCP were examined by a scanning electron microscope (SEM, JSM-6010LV, JEOL, Japan). The point of zero charge (pH_{pzc}) was evaluated by the equilibrium method (Su *et al.* 2011).

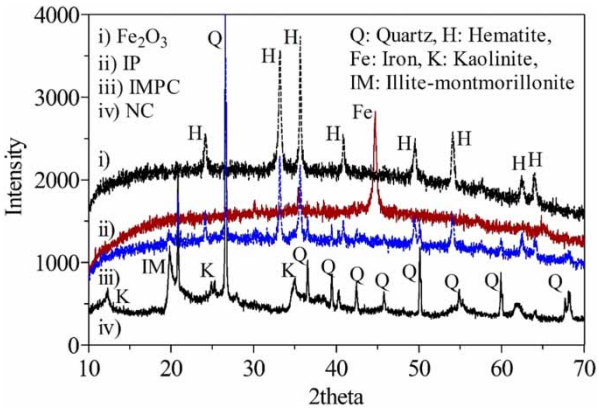

Figure 1 | The XRD patterns of IMCP and its constituents (NC, IP, and Fe_2O_3).

RESULTS AND DISCUSSION

Characterization of IMCP

The surface area, total pore volume, and average pore size of the adsorbent were 19.393 m^2/g, 0.0978 cm^3/g, and 20.169 nm, respectively. IMCP was mostly comprised of pore sizes within the range of 2–50 nm, implying that it was a mesoporous material according to the International Union of Pure and Applied Chemistry (IUPAC) classification (Kuila & Prasad 2013). The XRD patterns of IMCP and its constituent materials are illustrated in Figure 1. NC consists of quartz, kaolinite, and illite–montmorillonite. A single mineralogical phase was found for IP and Fe_2O_3, implying that these materials had a high purity. As expected, IMCP is comprised of mineralogical phases contributed by its constituent materials, indicating that NC successfully bound Fe_2O_3 and IP onto its surface. The adsorbent before adsorption appears to have a rough surface with flat non-unified shapes scattered around (Figure 2(a)). After adsorption, the surface feature has changed and created a concave morphology with spherical particles attached of various sizes (Figure 2(b)).

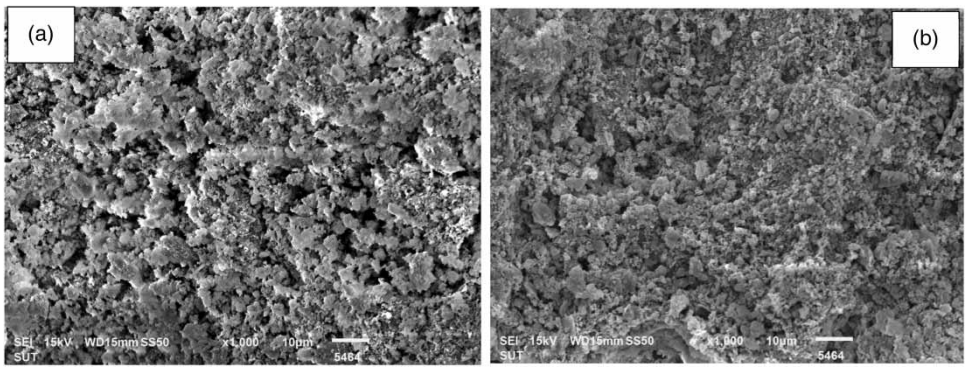

Figure 2 | The SEM analysis of IMCP (a) before and (b) after adsorption.

Batch experiments

Kinetic study

The interaction between the adsorbate and IMCP occurred at a fast pace for the first 12 h, and then gradually slowed down in the following 42 h (Figure 3). No significant improvement of the adsorption capacity was observed at 52 h, later considered to be the equilibrium contact time. The initial rapid uptake rate is due to the widely available active binding sites, particularly the external surface. Continuous filling of the active sites by the metal ions resulted in the slow reaction rate, diffusion phenomenon into the interior parts, and equilibrium. The kinetic experimental data were modelled by Equations (4) and (5), respectively:

$$\text{Pseudo-first order:} \quad Q_t = Q_e(1 - e^{k_1 t}) \tag{4}$$

$$\text{Pseudo-second order:} \quad Q_t = \frac{k_2 Q_e^2 t}{1 + k_2 Q_e t} \tag{5}$$

where t (h) is the amount of contact time, Q_t (μg/g) is the adsorption capacity at a certain time, and k_1 (1/h) and k_2 (g/μg/h) are the rate constants of the pseudo-first-order and pseudo-second-order models, respectively. The value of the correlation coefficient (R^2) and the closeness between the calculated equilibrium uptake ($Q_{e,cal}$) and experimental equilibrium uptake ($Q_{e,exp}$) were used for selecting the most suitable model. Table 1 indicates that the pseudo-second-order model better fitted the kinetic experimental data.

Table 1 | Kinetic parameters with experimental equilibrium capacity, $Q_{e,exp} = 497.01$ μg/g

Models	Parameters	Values
Pseudo-first order	$Q_{e,cal}$(μg/g)	467.2
	k_1(1/h)	0.2684
	R^2	0.9481
Pseudo-second order	$Q_{e,cal}$ (μg/g)	513.48
	k_2(g/μg/h) × 10^{-4}	7.585
	R^2	0.9818

Isotherm study

Increase in the initial adsorbate concentration led to an increase in the uptake capacity of IMCP (Figure 4). High concentration of the metal ions provides a low proportion of binding sites for the amount of the adsorbate, resulting in enhancing the interaction between the ions and adsorbent (Kango & Kumar 2016). To predict the equilibrium adsorption data, the Langmuir–Freundlich isotherm model was applied and it can be expressed by Equation (6):

$$\text{Langmuir} - \text{Freundlich model:} \quad Q_e = \frac{Q_m K_{L-F} C_e^{1/n}}{1 + K_{L-F} C_e^{1/n}} \tag{6}$$

where C_e (mg/L) is the adsorbate concentration at equilibrium, Q_e (mg/g) is the adsorption capacity at equilibrium, Q_m(mg/g) is the maximum adsorption capacity, K_{L-F} (L/mg) is the model constant, and $1/n$ is the heterogeneity factor. The obtained value of R^2 of the applied model was 0.9919, and this implied that the isotherm data were well described by the model. This suggests that the ions

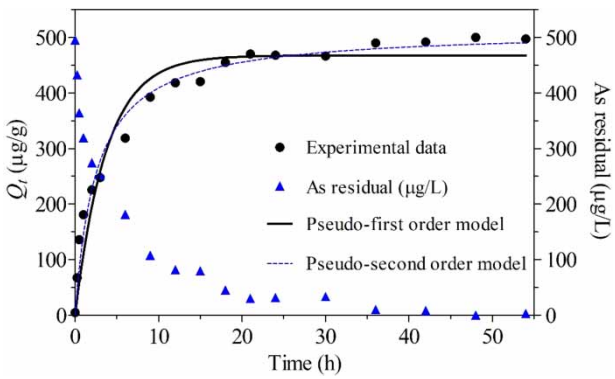

Figure 3 | The influence of contact time and fitting of the kinetic models.

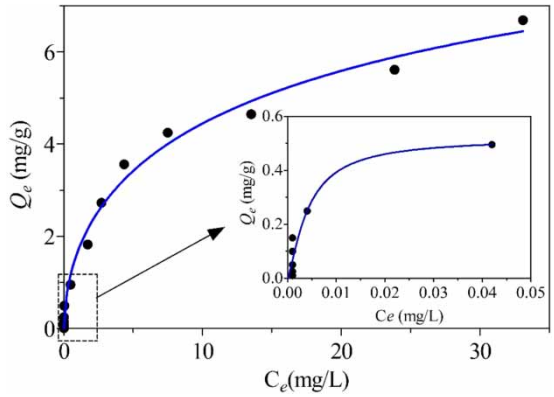

Figure 4 | The effect of initial adsorbate concentration and fitting of the isotherm model.

adsorbed onto the surface of IMCP involved both a homogeneous monolayer and heterogeneous complex surface feature (Chen *et al.* 2012). The maximum arsenic removal capacity, the model constant, and the heterogeneity factor were found to be 12.19 mg/g, 0.1585 L/mg, and 0.5596, respectively. This uptake capacity was higher than that of some porous adsorbents: 4.0 mg-As(III)/g and 4.50 mg-As(V)/g for iron–ceramic pellets (Shafiquzzam *et al.* 2013), 5.32 mg-As(V)/g for porous ceramic sorbent (Chen *et al.* 2012), 8.449 mg-As(V)/g for iron impregnation porous ceramic sorbent (Chen *et al.* 2012), and 11.52 mg-As(III)/g for zeolite-supported nanoscale zero-valent iron (Li *et al.* 2018). To evaluate the adsorption capacity at the lower arsenic concentration that is important for the application of treating arsenic-polluted water for a drinking purpose, the experimental isotherm data at lower equilibrium concentrations (<0.05 mg/L) was investigated (Figure 4), and the obtained mathematical expression of the model is as follows:

$$Q_e = \frac{0.5197 \times 1{,}370.05 C_e^{1.322}}{1 + 1{,}370.05 C_e^{1.322}} \quad (7)$$

Using the obtained equation, the adsorption capacity of IMCP at the 0.01 mg/L equilibrium concentration was found to be 0.393 mg/g, relatively lower than the experimental equilibrium capacity (0.497 mg/g) from the kinetic experiment (Table 1). This is likely true because the obtained value of R^2 was found to be 0.9250, indicating a fairly good performance of the fitting model.

Effect of initial solution pH

Figure 5 presents the influence of initial solution pH on the adsorption efficiency of IMCP with the initial adsorbate concentration of 0.5 mg/L. Higher adsorption efficiency of IMCP was observed in the acidic pH range. The efficiency decreased noticeably when the solution reached a pH greater than 8. In the alkaline condition (pH > 10), the adsorbent exhibited a dramatic reduction in removing the solutes from the solution. The solution pH affects the speciation of the metal ions, as well as the surface characteristics of the adsorbent. In natural water, As(III) species occur as: H_3AsO_3 (pH < 9.2), $H_2AsO_3^-$ (9 < pH < 12), $HAsO_3^{2-}$ (12 < pH < 13), and AsO_3^{3-} (pH > 13), and As(V) mainly exists in water as H_3AsO_4 at pH less than 2.2, $H_2AsO_4^-$ at pH between 2.2 and 6.98, $HAsO_4^{2-}$ at pH between 6.98 and 11.5, and AsO_4^{3-} at pH above 11.5 (Mohan & Pittman 2007). The surface of the adsorbent is more positively charged for pH lower than pH_{pzc} and predominates with the negative charge for $pH > pH_{pzc}$ (Chang *et al.* 2010). The proposed active surface sites of IMCP can be expressed as follows:

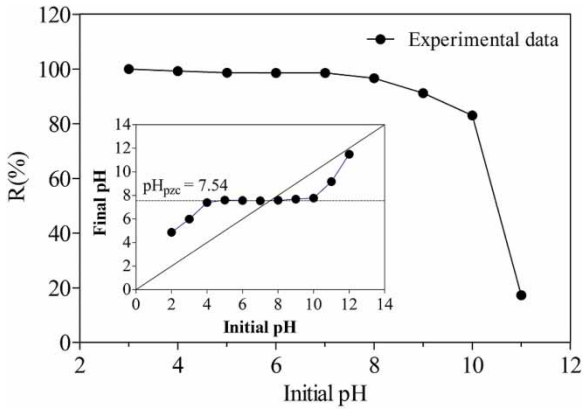

Figure 5 | The effect of initial solution pH and the point of zero charge of IMCP.

$$M \cdot Fe - OH_{(s)} + H^+ \leftrightarrow M \cdot Fe - OH_{2(s)}^+ \quad (pH < pH_{pzc})$$

$$M \cdot Fe - OH_{(s)} \leftrightarrow M \cdot Fe - O_{(s)}^- + H_{(aq)}^+ \quad (pH > pH_{pzc})$$

The final pH from the equilibrium method provided a plateau line at 7.54, corresponding to the value of pH_{pzc} (Figure 5), and obviously, the unfavorable electrostatic interaction or the electrical repulsion between the adsorbent and the adsorbate resulted in less adsorption efficiency at the basic pH range.

Effect of coexisting anions

Figure 6 shows the results of the adsorption efficiency onto IMCP in the presence of anions such as nitrate (NO_3^-), sulfate (SO_4^{2-}), and phosphate (PO_4^{3-}), representing univalent, bivalent, and trivalent anions that commonly exist in water. Increase in the amount of NO_3^- led to a slight reduction of the adsorbate adsorption efficiency, whereas an increase of SO_4^{2-} anions exhibited a quite noticeable

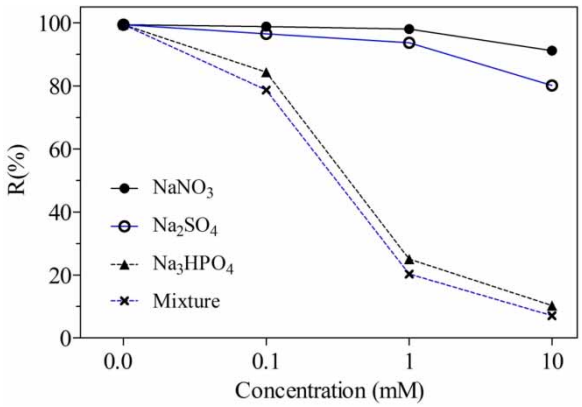

Figure 6 | The effect of coexisting anions on the adsorption efficiency of IMCP.

decrease in removing the metal ions from the solution. An extremely adverse effect was observed in the case of PO_4^{3-}. At a phosphate concentration of 10 mM, the metal ions were almost completely unable to be adsorbed. The reduction of the removal efficiency in the presence of anions could be explained by the occurrence of competition for the active sites. Phosphate and arsenic are in the same elemental group, providing similarities in chemical properties (Maliyekkal *et al.* 2009). Plus, phosphate easily forms an inner-sphere complex and more strongly attaches to iron(oxy)hydroxides than arsenic (Hsu *et al.* 2008).

Fixed-bed column experiments

The adsorbate removal performance in the fixed-bed column was analyzed by breakthrough curves expressed in terms of C_t/C_o ratio (C_t is the effluent concentration at a certain period and C_o is the influent concentration) against time (t). The breakthrough time (t_b) and saturation time (t_s) were selected when the instantaneous effluent concentration reached 0.01 mg/L and 95% of the influent concentration, respectively. The breakthrough curves obtained from the experiments are presented in Figure 7.

The breakthrough time and saturation time were shorter at higher feeding rate and extended at lower flow rate (Figure 7(a)). With an increase of the flow rate from 12.5 to 20.5 mL/min, the breakthrough time decreased from 36.52 to 4.08 h and the saturation time reduced from 141.29 to 56.53 h, and consequently, the saturated adsorption capacity of IMCP decreased from 312.59 to 139.59 μg/g (Table 2). Lower influent flow rate provided

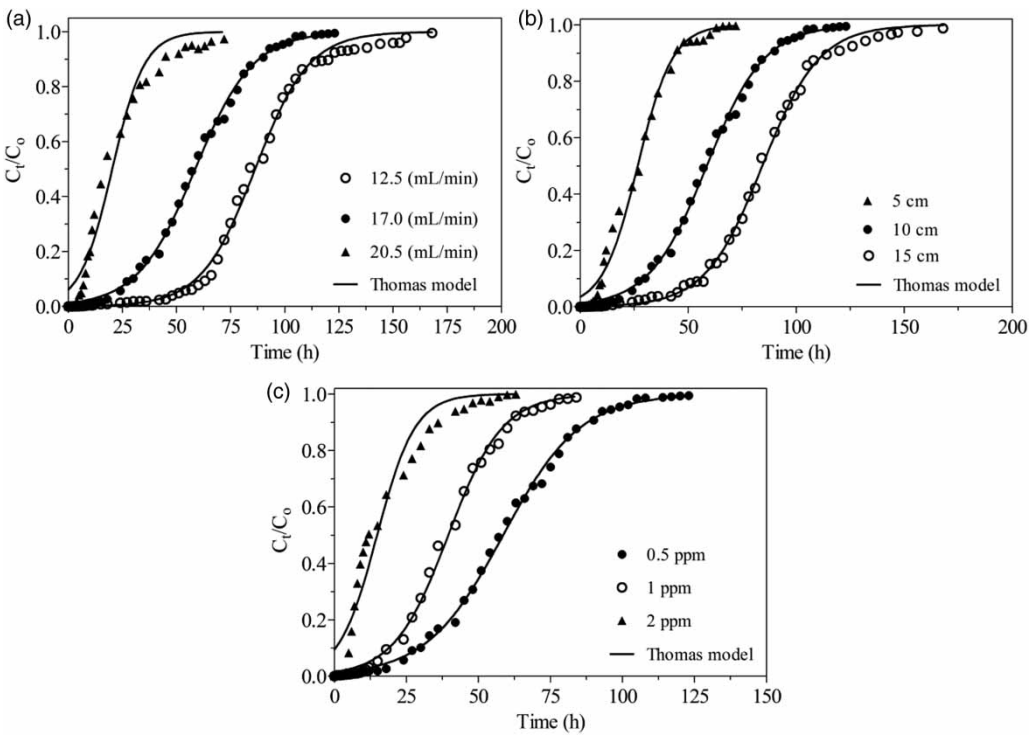

Figure 7 | Breakthrough profiles at a variation of (a) influent feeding flow rates, (b) adsorbent bed heights, and (c) initial concentrations.

Table 2 | Design parameters and the parameters of the Thomas model in the fixed-bed column

													Thomas model		
C_o (mg/L)	Q (mL/min)	H (cm)	pH	M (g)	υ (cm/min)	EBCT (min)	t_b (h)	t_s (h)	q_b (μg/g)	q_s (μg/g)	V_b (L)	BV	K_{Th} (L/h/mg)	q_o (μg/g)	R^2
0.5	12.5	10	7	95.94	0.95	10.53	36.52	141.29	134.18	312.59	27.39	208.09	0.1608	337.14	0.9968
0.5	17	10	7	95.94	1.29	7.75	15.59	97.63	77.94	284.62	15.90	120.70	0.1499	311.46	0.9984
0.5	20.5	10	7	95.94	1.55	6.45	4.08	56.53	24.67	139.59	5.02	37.95	0.2688	130.11	0.9718
0.5	17	5	7	47.97	1.29	3.88	5.99	57.64	60.07	253.95	6.11	92.63	0.2484	283.00	0.9912
0.5	17	10	7	95.94	1.29	7.75	15.59	97.63	77.94	284.62	15.90	120.70	0.1499	311.46	0.9984
0.5	17	15	7	143.91	1.29	11.63	25.30	134.75	84.54	303.97	25.81	130.52	0.1514	298.66	0.9984
0.5	17	10	7	95.94	1.29	7.75	15.59	97.63	77.94	284.62	15.90	120.70	0.1499	311.46	0.9984
1	17	10	7	95.94	1.29	7.75	7.44	70.98	74.70	384.67	7.59	57.60	0.1063	420.47	0.9973
2	17	10	7	95.94	1.29	7.75	2.24	45.4	67.96	314.35	2.28	17.34	0.0760	315.73	0.9530

Note: empty bed contact time (EBCT) = H/linear flow rate (υ); bed volume (BV) = volume water treated (V_b)/adsorbent bed volume in L.

the system with longer contact time (EBCT = 10.53 min) that allowed the metal ions access to more available binding sites of the adsorbent (Cruz-Olivares *et al.* 2013), resulting in a gradual occupancy of the solute towards the saturation point and higher adsorption capacity. At higher flow rate, the metal ions had insufficient residence time (EBCT = 6.45 min) for effectively interacting with active sites and/or diffusing into the pores (Jain *et al.* 2013), leading to the steeply inclined breakthrough profiles, as well as lower adsorption capacity.

The breakthrough profiles were observed to have a lower slope for a higher bed height, implying that a slow attainment of both breakthrough time and saturation time was achieved (Figure 7(b)). With an increase of the bed height from 5 to 15 cm, the breakthrough time and saturation time increased from 5.99 to 25.3 h and 57.64 to 134.75 h, respectively (Table 2). This could be attributed to the increased amount of the adsorbent and the long residence time for arsenic ions to stay in the system. Generally, at higher bed height, the sufficient interaction time (EBCT = 11.63 min) between the adsorbate and adsorbent leads to an increase in the adsorption capacity (Jang & Lee 2016). Increasing the bed height from 5 to 15 cm resulted in an increase of the saturated adsorption capacity of IMCP from 253.95 to 303.97 μg/g.

With a variation of initial arsenic concentrations, the breakthrough curve with a relatively flat S shape appeared far more to the right, and the curve shifted towards the left by changing to a steeply inclined S shape with increasing initial arsenic concentration (Figure 7(c)). With an increase of the initial concentration from 0.5 to 2 mg/L, the breakthrough time and saturation time decreased from 15.59 to 2.24 h and 97.63 to 45.4 h, respectively; however, within that variation of initial concentration from 0.5 to 2 mg/L, the saturated adsorption capacity increased from 284.62 to 384.67 μg/g (Table 2). The result can be explained by the fact that a higher initial concentration led to an increase in diffusion coefficient that consequently caused the metal ions to transport faster from the bulk solution to the IMCP surface, whereas a low initial concentration caused slower transport of the solutes to the binding sites and decreased the diffusion coefficient (Afroze *et al.* 2015).

In this study, the experimental data of the fixed-bed column were fitted with the Thomas model with the assumption that the adsorption follows the Langmuir isotherm and second-order kinetics. Its non-linear form can be expressed by Equation (8):

$$\frac{C_t}{C_o} = \frac{1}{1 + \exp\left(K_{Th} q_o M/Q - K_{Th} C_o t\right)} \tag{8}$$

where K_{Th} is the Thomas rate constant in L/h/mg, and q_o is the adsorption capacity in mg/g. Fitting the model to the breakthrough curves is shown in Figure 7. The correlation coefficient (R^2) of the Thomas model was found to be greater than 0.95; additionally, the calculated adsorption capacity of IMCP ranged from 139.59 to 384.67 μg/g,

comparable enough to the adsorption capacity (130.11–420.47 μg/g) obtained from the experiment (Table 2). This indicated that the Thomas model was really suitable for describing the column data. From Table 2, it also showed that 95.94 g of the adsorbent could produce the highest volume of water treated to below the permissible level of 10 μg/L at around 27 L, implying a better performance compared with some other adsorbents such as iron-oxide-coated natural rock (14.88 L) (Maji *et al.* 2012), porous table ceramic adsorbent and its iron-impregnated form (5.12–7.44 L) (Chen *et al.* 2012), and magnetic binary oxide particle adsorbent (7.85–8.64 L) (Dhoble *et al.* 2017).

CONCLUSIONS

The iron mixed clay porous pellet was developed for improving the quality of the aqueous solution coexisting with arsenite and arsenate in both static and dynamic systems. In the batch mode, the metal ion uptake rate onto the adsorbent surface occurred in multiple steps. The adsorbent was significantly influenced by varying initial solution pH and the presence of coexisting anions, especially a high initial pH value and phosphate anions. In the continuous fixed-bed mode, the adsorption had similar breakthrough curve patterns for the studied ranges of influent feeding flow rates, adsorbent bed heights, and initial adsorbate concentrations. The higher flow rate, lower initial concentration, and lower bed height would decrease the adsorption of arsenic onto the adsorbent in the fixed-bed column. IMCP is easily and economically produced and can be an effective low-cost composite adsorbent to improve the quality of arsenic-contaminated water. However, a pilot-scale experiment for treating natural arsenic-bearing water should be carried out.

ACKNOWLEDGEMENTS

The authors would like to gratefully thank the support from SUT-ASEAN Scholarship program, the Center for Scientific and Technological Equipment, and School of Environmental Engineering, Institute of Engineering, Suranaree University of Technology, Nakhon Ratchasima 30000, Thailand.

REFERENCES

Afroze, S., Sen, T. K. & Ang, H. M. 2015 Adsorption performance of continuous fixed bed column for the removal of methylene blue (MB) dye using *Eucalyptus sheathiana* bark biomass. *Research on Chemical Intermediates* **42** (3), 2343–2364.

Bhowmick, S., Chakraborty, S., Mondal, P., Van Renterghem, W., Van den Berghe, S., Roman-Ross, G., Chatterjee, D. & Iglesias, M. 2014 Montmorillonite-supported nanoscale zero-valent iron for removal of arsenic from aqueous solution: kinetics and mechanism. *Chemical Engineering Journal* **243**, 14–23.

Chakraborti, D., Das, B., Rahman, M. M., Nayak, B., Pal, A., Sengupta, M. K., Ahamed, S., Hossain, M. A., Chowdhury, U. K., Biswas, B. K., Saha, K. C. & Dutta, R. N. 2017 Arsenic in groundwater of the Kolkata Municipal Corporation (KMC), India: critical review and modes of mitigation. *Chemosphere* **180**, 437–447.

Chang, Q., Lin, W. & Ying, W. C. 2010 Preparation of iron-impregnated granular activated carbon for arsenic removal from drinking water. *Journal of Hazardous Materials* **184** (1–3), 515–522.

Chen, R., Zhang, Z., Lei, Z. & Sugiura, N. 2012 Preparation of iron-impregnated tablet ceramic adsorbent for arsenate removal from aqueous solutions. *Desalination* **286**, 56–62.

Cruz-Olivares, J., Pérez-Alonso, C., Barrera-Díaz, C., Ureña-Nuñez, F., Chaparro-Mercado, M. C. & Bilyeu, B. 2013 Modeling of lead (II) biosorption by residue of allspice in a fixed-bed column. *Chemical Engineering Journal* **228**, 21–27.

Dhoble, R. M., Maddigapu, P. R., Rayalu, S. S., Bhole, A. G., Dhoble, A. S. & Dhoble, S. R. 2017 Removal of arsenic(III) from water by magnetic binary oxide particles (MBOP): experimental studies on fixed bed column. *Journal of Hazardous Materials* **322**, 469–478.

Doušová, B., Grygar, T., Martaus, A., Fuitová, L., Koloušek, D. & Machovič, V. 2006 Sorption of As(V) on aluminosilicates treated with Fe(II) nanoparticles. *Journal of Colloid and Interface Science* **302** (2), 424–431.

Hsu, J. C., Lin, C. J., Liao, C. H. & Chen, S. T. 2008 Evaluation of the multiple-ion competition in the adsorption of As(V) onto reclaimed iron-oxide coated sands by fractional factorial design. *Chemosphere* **72** (7), 1049–1055.

Jain, M., Garg, V. K. & Kadirvelu, K. 2013 Cadmium(II) sorption and desorption in a fixed bed column using sunflower waste carbon calcium–alginate beads. *Bioresource Technology* **129**, 242–248.

Jang, J. & Lee, D. S. 2016 Enhanced adsorption of cesium on PVA-alginate encapsulated Prussian blue-graphene oxide hydrogel beads in a fixed-bed column system. *Bioresource Technology* **218**, 294–300.

Kango, S. & Kumar, R. 2016 Low-cost magnetic adsorbent for As(III) removal from water: adsorption kinetics and isotherms. *Environmental Monitoring and Assessment* **188** (1), 60.

Kuila, U. & Prasad, M. 2013 Specific surface area and pore-size distribution in clays and shales. *Geophysical Prospecting* **61** (2), 341–362.

Li, Z., Wang, L., Meng, J., Liu, X., Xu, J., Wang, F. & Brookes, P. 2018 Zeolite-supported nanoscale zero-valent iron: new findings on simultaneous adsorption of Cd(II), Pb(II), and As(III) in aqueous solution and soil. *Journal of Hazardous Materials* **344**, 1–11.

Maji, S. K., Kao, Y. H., Wang, C. J., Lu, G. S., Wu, J. J. & Liu, C. W. 2012 Fixed bed adsorption of As(III) on iron-oxide-coated natural rock (IOCNR) and application to real arsenic-bearing groundwater. *Chemical Engineering Journal* **203**, 285–293.

Maliyekkal, S. M., Philip, L. & Pradeep, T. 2009 As(III) removal from drinking water using manganese oxide-coated-alumina: performance evaluation and mechanistic details of surface binding. *Chemical Engineering Journal* **153** (1–3), 101–107.

Mohan, D. & Pittman Jr., C. U. 2007 Arsenic removal from water/wastewater using adsorbents: a critical review. *Journal of Hazardous Materials* **142** (1–2), 1–53.

Mohapatra, D., Mishra, D., Chaudhury, G. R. & Das, R. P. 2007 Arsenic(V) adsorption mechanism using kaolinite, montmorillonite and illite from aqueous medium. *Journal of Environmental Science and Health Part A* **42** (4), 463–469.

Sabbatini, P., Yrazu, F., Rossi, F., Thern, G., Marajofsky, A. & Fidalgo de Cortalezzi, M. M. 2010 Fabrication and characterization of iron oxide ceramic membranes for arsenic removal. *Water Research* **44** (19), 5702–5712.

Sdiri, A., Higashi, T., Hatta, T., Jamoussi, F. & Tase, N. 2011 Evaluating the adsorptive capacity of montmorillonitic and calcareous clays on the removal of several heavy metals in aqueous systems. *Chemical Engineering Journal* **172** (1), 37–46.

Shafiquzzam, M., Hasan, M. & Nakajima, J. 2013 Iron mixed ceramic pellet for arsenic removal from groundwater. *Environmental Engineering Research* **18** (3), 163–168.

Sharma, A. K., Tjell, J. C., Sloth, J. J. & Holm, P. E. 2014 Review of arsenic contamination, exposure through water and food and low cost mitigation options for rural areas. *Applied Geochemistry* **41**, 11–33.

Su, J., Huang, H. G., Jin, X. Y., Lu, X. Q. & Chen, Z. L. 2011 Synthesis, characterization and kinetic of a surfactant-modified bentonite used to remove As(III) and As(V) from aqueous solution. *Journal of Hazardous Materials* **185** (1), 63–70.

Te, B., Wichitsathian, B., Yossapol, C. & Wonglertarak, W. 2017 Development of low-cost iron mixed porous pellet adsorbent by mixture design approach and its application for arsenate and arsenite adsorption from water. *Adsorption Science and Technology* **36** (1–2), 372–392.

First received 29 October 2018; accepted in revised form 14 April 2019. Available online 29 April 2019